Atmos. Chem. Phys., 25, 10625–10641, 2025
https://doi.org/10.5194/acp-25-10625-2025

Atmospheric Chemistry and Physics
Open Access
EGU

On the presence of high nitrite (NO_2^-) in coarse particles at Mt. Qomolangma

Zhongyi Zhang[1], Chunxiang Ye[2], Yichao Wu[1], Tao Zhou[3], Pengfei Chen[4,5], Shichang Kang[4,5], Chong Zhang[2], Zhuang Jiang[1], and Lei Geng[1,3,6]

[1]National Key Laboratory of Deep Space Exploration/School of Earth and Space Sciences, University of Science and Technology of China, Hefei 230026, Anhui, China
[2]SKL-ESPC & SEPKL-AERM, College of Environmental Sciences and Engineering, and Center for Environment and Science, Peking University, Beijing 100871, China
[3]Deep Space Exploration Laboratory, Hefei, 230088, Anhui, China
[4]Key Laboratory of Cryospheric Science and Frozen Soil Engineering, Northwest Institute of Eco-Environment and Resources, Chinese Academy of Sciences, Lanzhou, 730000, Gansu, China
[5]University of Chinese Academy of Sciences, Beijing, 100049, China
[6]CAS Center for Excellence in Comparative Planetology, University of Science and Technology of China, Hefei 230026, Anhui, China

Correspondence: Lei Geng (genglei@ustc.edu.cn)

Received: 27 December 2024 – Discussion started: 16 January 2025
Revised: 30 July 2025 – Accepted: 31 July 2025 – Published: 17 September 2025

Abstract. Atmospheric reactive nitrogen cycling, with nitrous acid (HONO) and particulate nitrite (NO_2^-) as important intermediates, is crucial for maintaining the atmospheric oxidation capacity of background atmosphere on the Tibetan Plateau. During an 11 d field campaign at the Base Camp of Mt. Qomolangma in spring of 2022, we observed significant enrichments of NO_2^- in total suspended particulate (TSP) with a mean concentration of $375 \pm 386\ ng\ m^{-3}$, while NO_2^- was absent in fine particles ($PM_{2.5}$). The comparison revealed that NO_2^- predominately exists in coarse particles. Local surface soil at the sampling site also exhibited high levels of NO_2^-, with $\delta^{15}N$ value similar to NO_2^- in TSP. This isotopic similarity suggests that wind-blown soil is probably the primary source of NO_2^- in TSP, accounting for the background levels. While concentration changes of water-soluble inorganic ions in TSP and $PM_{2.5}$ in response to shifts in air mass back-trajectories imply that atmospheric pollutants transported from South Asia may further elevate the NO_2^-, the specific mechanisms of long-range transport resulting in NO_2^- accumulation in TSP rather than $PM_{2.5}$ remain unknown and need to be investigated. The elevated levels of TSP NO_2^- may readily participate in atmospheric reactive nitrogen cycling through gas-particle partitioning or photolysis, leading to the production of HONO, OH and NO and thereby influencing oxidation chemistry. Further efforts on the sources and atmospheric chemistry of particulate nitrite are warranted, particularly in the pristine Tibetan Plateau, where even small inputs of NO_x or HONO can disproportionately affect oxidant budgets and reactive nitrogen cycling.

Published by Copernicus Publications on behalf of the European Geosciences Union.

1 Introduction

The Tibetan Plateau (TP), known as the "Third Pole", represents one of the most climate-sensitive regions on Earth (Yao et al., 2012). Over recent decades, the TP has experienced significant and rapid climate warming, primarily driven by increasing aerosol loadings and greenhouse gas concentrations due to its geographic proximity to East Asia and South Asia with intensive anthropogenic emissions (Kang et al., 2019; Lau et al., 2010; Lüthi et al., 2015). Atmospheric oxidation capacity (AOC) regulates secondary aerosol formation and trace gases removal, including CH_4 (Wang et al., 2023; Ye et al., 2023, 2016; Andersen et al., 2023), therefore acting as a critical link between atmospheric pollution and regional climate warming. Previous studies have suggested that strong solar radiation, high ozone (O_3) and relatively high water vapor dominate the relatively strong AOC over the TP (Lin et al., 2008). Recent field campaign further highlighted the rapid reactive nitrogen cycling, with N(III) species (i.e., HONO) as the intermediate, also plays an important role in maintaining the strong AOC in TP (Wang et al., 2023). For example, Wang et al. (2023) reported high-than-expected HONO ($\sim 30 \pm 13$ pptv) in the Namco station, a representative background site in the central TP, with identified HONO sources including NO_2 heterogenous conversion, soil emission and particulate nitrate photolysis (Wang et al., 2023). Incorporating the observed HONO into model simulations approximately doubled the estimated OH abundance compared to simulations without HONO constraints. However, a detailed HONO budget analysis indicated these three dominant sources could not account for the observed high daytime HONO levels at the background site, implying the existence of additional, yet unidentified, HONO sources.

Particulate nitrite (NO_2^-) likely represents a potential source of HONO through thermodynamic partitioning processes under favorable atmospheric conditions, provided particulate nitrite is present in significant amounts (VandenBoer et al., 2014a; Chen et al., 2019; Li, 2012). Interestingly, relatively high levels of nitrite in total suspended particulate (TSP) have also been reported from remote sites of TP, i.e., in a forest site in the Southeast Tibet ($\sim 140\,\mathrm{ng\,m^{-3}}$) and at the Qomolangma monitoring station (QOMS, $\sim 60\,\mathrm{ng\,m^{-3}}$) (Bhattarai et al., 2019, 2023). Such high levels of particulate nitrite may also contribute to the strong AOC in TP, either via directly photolysis to produce NO_x (Jacobi et al., 2014) or indirectly serve as an important source of HONO through gas-particle partitioning (Reaction R1). However, the sources and formation mechanisms for the relatively high level of atmospheric NO_2^- observed in the TP remain unclear.

$$HONO_{(g)} \leftrightarrow HONO_{(aq)} \leftrightarrow NO^-_{2(aq)} + H^+_{(aq)} \quad \text{(R1)}$$

The stable nitrogen and oxygen isotopic compositions ($\delta^{15}N$, $\delta^{18}O$, and $\Delta^{17}O$; where $\delta = (R_{sample}/R_{reference} - 1) \times 1000\,‰$ and with R denoting the $^{15}N/^{14}N$, $^{18}O/^{16}O$, and $^{17}O/^{16}O$ ratios; $\Delta^{17}O = \delta^{17}O - 0.52 \times \delta^{18}O$) may provide diagnostic information regarding the sources and formation pathways of atmospheric nitrite. Similar isotopic approaches have been widely used to explore the nitrate (NO_3^-) sources (Morin et al., 2008; Zong et al., 2020; Geng et al., 2014; Fang et al., 2011; Hastings et al., 2003; Zhang et al., 2022, 2021b; Liu et al., 2018; Felix and Elliott, 2014; Miller et al., 2018). Considering that atmospheric NO_2^- may share similar sources and formation pathways with NO_3^-, the specific NO_2^- formation pathways are expected to be characterized by distinct oxygen or nitrogen isotopic endmembers, despite reports on the atmospheric NO_2^- isotopic compositions are rare. For instance, NO_2^- produced from the photolysis of particulate NO_3^- may possess very negative $\delta^{15}N$ values compared to NO_3^-, analogous to the pronounced nitrogen isotope fractionation effects associated with snow nitrate photolysis (Erbland et al., 2013; Frey et al., 2009), while the $\Delta^{17}O$ of NO_2^- is expected to closely resemble that of NO_3^- as the oxygen atom in NO_2^- is imparted from NO_3^-, unless significant oxygen atom exchange between NO_2^- and aerosol water occurs. The $\Delta^{17}O$ of NO_2^- (and HONO) from primary emission sources is expected to be negligible, while that generated from heterogeneous reactions of NO_2 on the aerosol surface would be characterized by positive $\Delta^{17}O$ values depending on the degree of NO_2^- and aerosol water oxygen isotope exchange. These unique isotopic fingerprints may be utilized in distinguishing the sources and formation pathways of atmospheric NO_2^-.

To gain insight into the sources and/or formation mechanisms of atmospheric NO_2^- in the pristine environment of TP, we collected the TSP and fine particulate matter ($PM_{2.5}$) synchronously at the Base Camp, the north slope of the Mt. Qomolangma during the campaign of "Earth Summit Mission-2022" scientific expedition from 24 April to 6 May 2022, with additional surface soil samples collected in May 2023. The NO_2^- concentration and multi-isotopic signatures ($\delta^{15}N$, $\delta^{18}O$, and $\Delta^{17}O$) in aerosol and surface soil were then determined in order to evaluate the potential sources of atmospheric NO_2^-. Additionally, the potential environmental implication of atmospheric nitrite was explored in the term of atmospheric oxidation capacity at this pristine environment.

2 Material and Method

2.1 Site description

The Base Camp is located in the middle of the Rongbuk valley (86.85° E, 28.14° N), situated ~ 5200 m above sea level (m a.s.l.) on the north slope of the Mt. Qomolangma (Zou et al., 2008; Zhu et al., 2006). The surrounding surface consists of loosed soil, gravel, broken rocks of various sizes, with sparse vegetation due to the semi-arid status (Ming et al., 2007; Zou et al., 2008). Rongbuk valley is characterized by a depth of ~ 1000 m and a floor width of ~ 1000 m, with elevations of the surrounding mountains exceeding 6000 m on both sides (Zou et al., 2008). Attributed to the unique to-

pography, the local air circulation is dominated by mountain and valley breezes. The predominant wind regime is the katabatic flow of southerly and southeasterly, which is typically persists from noon to midnight (Zhu et al., 2006; Zou et al., 2008; Zhou et al., 2011). The nearest accessible area for residents and visitors is at least 2 km north of the Base Camp. During the campaign, electricity and natural gases were routinely used for cooking and hot water production. There were intermittent vehicle exhaust emissions around the station during daytime for the daily necessaries supporting, i.e., water and food. To minimize the influence of local anthropogenic activities on sampling, the instruments were set in the southeast (upwind direction, Fig. S1 in the Supplement) and approximately 100 m away from the living space of the Base Camp. The anthropogenic influence on the sampling is expected to be minimal.

2.2 Field campaign and sample collection

From 26 April to 6 May 2022, TSP samples were collected simultaneously with NO_2 using a homemade denuder-filter system (Zhou et al., 2022). A similar system has been widely used to separately collect atmospheric particulate matter and N-containing gases for isotopic analysis (Chai et al., 2019, 2021), suggesting the mutual interference between the particulate and gaseous phases to be minimal. A polytetrafluoroethylene (PTFE) sleeve is used to assemble the homemade denuder with the filter pack, flowmeter, and pump. The filter pack was placed in the front of the denuder. All connections between the various parts of the sampling apparatus are made using $3/8''$ Teflon tubing. A detailed description of the sampling apparatus can be found in our previous report (Zhou et al., 2022). Whatman quartz filter (circles, diam. 47 mm, pre-heated at 400 °C for 3 h before use) was placed into the filter pack to collect TSP sample. In the present study, the collected bulk aerosol can be regarded as TSP since no size-selective inlet was employed. The flow rate was controlled at 30 L min^{-1} using a flowmeter. Previous reports have indicated that the flow rate has negligible effect on the concentrations of sulphate, nitrate, and ammonium when using quartz filter for sampling (Keck and Wittmaack, 2005). To minimize the potential influence of the loose ground surface on the TSP collection, a mountain tent was used to separate the pump (out the tent) with the denuder-filter system (in the other side of tent), and the inlet Teflon tube was stretched out of the tent for ∼ 1.5 m height straight.

From 24 April to 6 May 2022, $PM_{2.5}$ were sampled using a high-volume aerosol sampler (TH-1000F; Wuhan Tianhong Instruments Co. Ltd., China) equipped with $PM_{2.5}$ inlet and Whatman quartz-fiber filters (sheets, 203 mm × 254 mm) at a flow rate of 1.5 m^3 min^{-1}. All the quartz filters were pre-heated at 400 °C for 3 h before use. In general, TSP and $PM_{2.5}$ samples were collected with diurnal resolution during this campaign, with daytime samples from approximately 09:00–20:00 and nighttime samples from 21:00–08:00 (local time), respectively. From 2 to 4 May, we collected the daytime TSP and $PM_{2.5}$ samples in the morning (09:00–14:00) and afternoon (14:00–20:00), respectively. A total of 24 TSP samples (including 2 blanks) and 29 $PM_{2.5}$ (including 3 blanks) were collected during this campaign. After each sampling period, quartz filters were removed from the filter pack/$PM_{2.5}$ inlet and immediately wrapped in pre-baked aluminum foil and then stored in frozen until analysis to minimize potential loss of nitrite. During the campaign, snowfall events occurred on the night of 29 April and during the daytime of 30 April.

Surface soil samples (0–5 cm depth, $n = 9$) were collected in May 2023 from the east slope, west slope and south sides of the Rongbuk valley. A polytetrafluoroethylene (PTFE) shovel was used to collect soil. The collected soil was immediately transferred to clean plastic bags, sealed and kept frozen. Soil samples were transported into laboratory using a cold chain. Upon arrival at our laboratory, the soil samples were passed through a 60-mesh screen (∼ 0.25 mm) to remove larger particles and thoroughly homogenized prior to chemical and isotopic analysis.

2.3 Ionic concentration analysis and uncertainty estimation

Water-soluble inorganic ions (WSIs, including Na^+, NH_4^+, K^+, Mg^{2+}, Ca^{2+}, Cl^-, NO_2^-, NO_3^-, and SO_4^{2-}) in TSP (entire filter, ∼ 16.6 cm^2) and $PM_{2.5}$ (1/32 section, ∼ 13.0 cm^2) were extracted using 20 mL Milli-Q ultrapure water (18.2 Ωcm) in an ultrasonic bath at room temperature for 30 min. Note the TSP filters were cut to fit the filter holder from the standard Whatman quartz-fiber filters which were also used as the $PM_{2.5}$ filters. After filtration through a 0.22 µm pore size syringe filter which was pre-cleaned with ultrapure water, the filtrate was subjected to inorganic species analysis using ion chromatography (Dionex Aquion) (Zhang et al., 2020). Blank filters were pretreated and measured the same as real samples, and the limits of detection (LOD) was calculated as 3 times of standard deviations of blanks (Fang et al., 2015a). In general, Na^+ in the blank filters is comparable to samples, a well-known issue for the Whatman quartz filter which is high in Na^+ blank. Therefore, in this study, we discarded the Na^+ data. The volatile components (i.e., NH_4^+, NO_2^-, NO_3^-) and K^+ in blank are low but several times higher than the detection limits; SO_4^{2-}, Mg^{2+} and Ca^{2+} in blank are significantly higher than the respective LOD but lower than samples by at least five times (the lower end). All reported concentrations of each ion were blank corrected as follows:

$$C_i = \frac{(\rho_{\text{sample}} - \rho_{\text{blank}}) \times V_{\text{water}} \times F}{V_{\text{air}}} \quad (1)$$

with C_i representing the ambient concentrations of specie i in air (ng m^{-3} or µg m^{-3}), ρ_{sample} and ρ_{blank} are the concentrations determined by the ion chromatography (ng mL^{-1}), V_{water} is the volume of ultrapure water used for extraction

(20 mL), V_{air} is the volume of air sampled for each $PM_{2.5}$ or TSP filter, F is the ratio of particulate matter collection area for $PM_{2.5}$ or TSP filters to the filter area used for extraction.

The overall uncertainty in ion concentration was estimated according to the law of error propagation, accounting for the sampling air volume (3 % for $PM_{2.5}$ samples and 1 % for TSP samples as provided by the manufactures), the extraction of water volume (~ 0.3 % for pipetting from the manufacture Eppendorf), the blanks, and the analytical uncertainty from ion chromatography and calibration, assuming that these factors are independent. The analytical uncertainty for water-soluble ions concentration determination using ionic chromatography has been extensively assessed in our laboratory, with values typically < 5 % for all inorganic species at concentration of 500 ng mL^{-1}. The combined uncertainty about the ionic concentrations in $PM_{2.5}$ and TSP are shown in Table S1 in the Supplement. In general, TSP samples are associated with relatively high overall uncertainty compared to $PM_{2.5}$ samples, perhaps due to the relatively high blank variability from the low mass loadings in TSP.

For soil ionic concentration analysis, 4.0 g sieved soil was extracted using 20 mL Milli-Q ultrapure water, shaken for 30 min at room temperature. After centrifugation, the extract was passed through 0.45 mm filters before ions analysis. The concentration determination of water-soluble inorganic ions in soil extract was similar to that of aerosol samples. Detailed procedure for the extraction of soil inorganic ions, especially the NO_2^- has been descried in previous report (Homyak et al., 2015).

2.4 Isotopic analysis

After concentration measurements, isotopic analyses ($\delta^{15}N$, $\delta^{18}O$, and $\Delta^{17}O$) of NO_2^- in TSP were conducted using the azide method (Casciotti et al., 2007). The azide method can reduce nitrite ion in solution into N_2O in a single step, while nitrate ion remains unchanged, ensuring no interference on the nitrite isotopic analysis. The azide reagent is prepared by mixing 2 M sodium azide with 40 % acetic acid at a 1 : 1 ratio by volume in our laboratory. NO_2^- standards and samples were pretreated under identical conditions concerning the total volume, nitrite amount, water isotope, and matrix. The $\delta^{15}N$, $\delta^{18}O$, and $\delta^{17}O$ of N_2O reduced from NO_2^- in the TSP samples and standards were determined using a Finnigan® MAT253 plus isotope ratio mass spectrometer (IRMS) equipped with a GasBench II and preconcentration system. The data calibration followed the procedures described in Albertin et al. (2021), using three international KNO_2 salt standards (RSIL-N10219, RSIL-N7373, and RSIL-N23 with respective $\delta^{15}N$ and $\delta^{18}O$ values of 2.8 ‰/88.5 ‰, −79.6 ‰/4.2 ‰, and 3.7 ‰/11.4 ‰). The $\Delta^{17}O$ values of the three international references have not been certified. To address this, a series laboratory experiments was conducted to determine the true values of three international references in our laboratory (Zhang et al., 2025). In brief, each nitrite international reference was oxidized into NO_3^- by O_3 produced from commercial ozone generator. A parallel flow of O_3 was also used to convert a normal KNO_2 salt ($\Delta^{17}O = 0$) into NO_3^- to quantify the $\Delta^{17}O$ transfer during O_3 oxidation, following the approach of (Vicars and Savarino, 2014). Based on these experiments, the $\Delta^{17}O$ of RSIL-N7373 and RSIL-N23 are determined to be negligible, consistent with previous findings (Albertin et al., 2021), while the $\Delta^{17}O$ of RSIL-N10219 is determined to be (-9.3 ± 0.2) ‰ in our laboratory. The ^{17}O-excess in samples is then calculated as $\Delta^{17}O = \delta^{18}O - 0.52 \times \delta^{17}O$. The standard deviations for $\delta^{15}N$, $\delta^{18}O$, $\Delta^{17}O$ of reference materials ($n = 10$) were determined to be less than 0.1 ‰, 0.6 ‰, and 0.4 ‰, respectively.

For soil NO_2^- isotopic analysis, ~ 30.0 g sieved soil was extracted using 150 mL Milli-Q ultra-pure water. The soil extract was then preconcentrated into 10 mL using ion-exchange resin before isotopic analysis. The preconcentration approach was widely used for nitrate isotopic analysis in snow and ice samples, and the detailed procedures and the performance have been provided in Erbland et al. (2013) and evaluated in our laboratory (Sect. S1 in the Supplement). The concentrated soil extracts (50 nmol NO_2^-) was then subjected to soil NO_2^- isotopic analysis by converting into N_2O via the azide method. For soil NO_3^- isotopic analysis, ~ 5.0 g sieved soil was extracted with 15 mL of 2 M KCl solution (Fang et al., 2015b). The remaining procedures of soil NO_3^- and NO_2^- analysis were same as those for TSP samples, as aforementioned.

2.5 Complementary analyses of air mass backward trajectory

To evaluate the possible impact of biomass burning emissions or other pollution sources from South Asia, the Hybrid Single-Particle Lagrangian Integrated Trajectory (HYSPLIT) model (performed using TrajStat plugin of the MeteoInfo software) and archived Global Data Assimilation System (GDAS) of meteorological data were used to model the air mass back trajectories (Wang, 2014). In this study, 3 d air mass backward trajectories with arriving height of 1000 m above ground level were simulated to identify the most likely pathway and potential source regions of the air masses at the Base Camp (Bhattarai et al., 2023; Lin et al., 2021). Moreover, the Fire Information and Resource Management System (FIRMS) developed by Moderate Resolution Imaging Spectrometer (MODIS) (https://worldview.earthdata.nasa.gov, last access: 7 September 2024) was employed to identify the distribution of active fire spots during the sampling period.

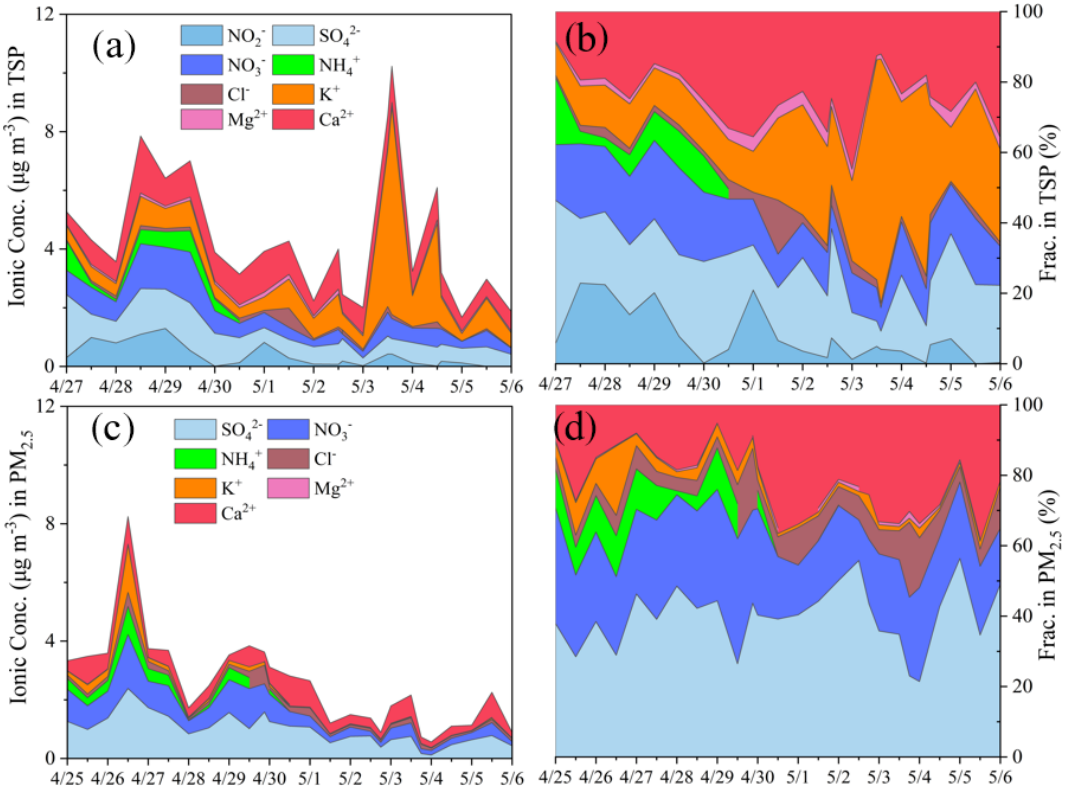

Figure 1. The chemical compositions and time series of mass concentrations of water-soluble inorganic species (NO_2^-, SO_4^{2-}, NO_3^-, Ca^{2+}, etc.), as well as the corresponding mass fractions in respective TSP **(a, b)** and $PM_{2.5}$ **(c, d)** samples collected at Base Camp of Mt. Qomolangma in spring 2022.

3 Results

3.1 Mass concentrations of water-soluble inorganic ions in TSP and $PM_{2.5}$

Figure 1 displays the chemical compositions of water-soluble inorganic ions, their corresponding time series and fractional contributions in TSP and $PM_{2.5}$. Throughout the campaign, substantial variations of total WSIs in $PM_{2.5}$ and TSP were observed. For $PM_{2.5}$ samples, the mass concentrations of total WSIs before 30 April were higher than that from 1 to 6 May (4.1 ± 1.7 versus $1.7 \pm 0.6\,\mu g\,m^{-3}$; $p < 0.05$). The cut-off date of 30 April was selected based on observed shifts in concentrations of water-soluble ions and air mass origins (described in Sect. 4.2). This decline of total WSIs after 30 April was predominately driven by significant reductions in secondary inorganic species, i.e., SO_4^{2-}, NO_3^- and NH_4^+, with the magnitude by more than 60 %. In particular, NH_4^+ in $PM_{2.5}$ was on average $(322 \pm 243)\,ng\,m^{-3}$ before 30 April whereas NH_4^+ in $PM_{2.5}$ collected during daytime and nighttime of 1 May were 1 and 3 $ng\,m^{-3}$, respectively, and NH_4^+ in $PM_{2.5}$ extractions from 2 to 6 May was below the detection limit. Therefore, the fractional contribution of secondary inorganic species in $PM_{2.5}$ also decreased (Fig. 1d). Similarly, K^+ in $PM_{2.5}$, a good tracer of biomass burning (Ma et al., 2003), also declined significantly after 30 April (269 ± 432 versus $22 \pm 12\,ng\,m^{-3}$; $p < 0.05$). The elevated concentrations of WSIs before 30 April ($4.1 \pm 1.7\,\mu g\,m^{-3}$) are comparable to previous reports at QOMS station ($4.2 \pm 2.2\,\mu g\,m^{-3}$) in the spring (Lin et al., 2021). In comparison, concentrations of Ca^{2+} and Mg^{2+}, tracers of wind-blown dust (Wang et al., 2002), decreased by less than 20 % after 30 April. In general, SO_4^{2-}, NO_3^-, and Ca^{2+} are the most abundant species in $PM_{2.5}$, accounting for the majority of the mass of total WSIs. In addition, no clear diurnal variation of water-soluble inorganic ions in $PM_{2.5}$ was observed in this study (Fig. S2).

Some water-soluble inorganic ions (e.g., SO_4^{2-}, NO_3^- and NH_4^+) in TSP showed similar variation trends with that in $PM_{2.5}$ throughout the campaign, while others, such as K^+, exhibited divergent behavior (Fig. 1). For example, after 30 April, the secondary inorganic species in TSP declined considerably by over 50 % (i.e., NH_4^+ in TSP declined by more than tenfold), while Ca^{2+} in TSP decreased with a smaller degree (< 15 %) and Mg^{2+} remained stable. In contrast, TSP K^+ (from both crustal and biomass burning sources) (Hsu et al., 2009) drastically surged on 3 and 4 May. Note that other species in TSP, i.e., SO_4^{2-} and NO_3^- also increased to some extent on 3 May. The time series of water-soluble inorganic ions in the coarse-mode particulate, cal-

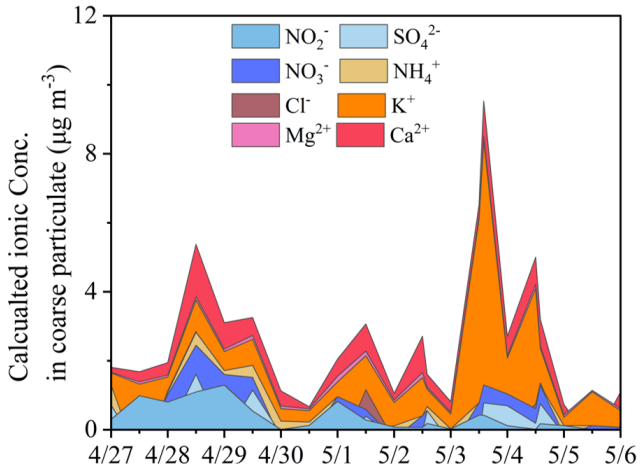

Figure 2. The estimated chemical compositions and time series of mass concentrations of chemical species (NO_2^-, SO_4^{2-}, NO_3^-, Ca^{2+}, etc.) in coarse-mode particulate during the springtime campaign (calculated as the difference between TSP and $PM_{2.5}$). Discontinuities in the time series were observed for certain species (e.g., SO_4^{2-}), likely resulting from relatively lower concentrations in the TSP samples compared to those in the corresponding $PM_{2.5}$ samples. This discrepancy is likely attributed to the propagated uncertainties involved in the concentration analysis, sampling approach and blank corrections.

culated as the differences between TSP and $PM_{2.5}$, are presented in Fig. 2. Due to the overall analytical uncertainties, the air concentrations of SO_4^{2-} in $PM_{2.5}$ samples occasionally exceeded that in corresponding TSP samples on some days.

Figure 3 presents the ion balance of measured water-soluble ions in $PM_{2.5}$ throughout the campaign as well as in TSP collected before and after 30 April, respectively, to highlight the significant decline in TSP NO_2^-. There is a strong correlation between cation and anion equivalents in $PM_{2.5}$ samples ($R^2 = 0.70$), whereas the correlations decreased in TSP samples ($R^2 = 0.46$ before 30 April and 0.49 after that, respectively). The nanogram-equivalent weights of cation were significantly higher than that of anions for all samples, with ratio of cation to anion equivalent of ~ 1.5 for $PM_{2.5}$, ~ 1.9 for TSP collected before 30 April, ~ 4.2 for TSP collected after 1 May. Clearly, the declines in TSP NO_2^- after 30 April resulted in relatively higher cation/anion equivalent ratio. The slopes of the correlation lines exceeded unity for $PM_{2.5}$ and TSP samples, indicating the alkaline nature of aerosol. The observed deficiency of anion can be attributed to the presence of carbonates (i.e., $CaCO_3$), which can dissolve in water during extraction to release CO_3^{2-} and/or HCO_3^- despite the relatively low solubility (Zhang et al., 2021a).

The most distinct feature of chemical compositions in TSP was the elevated level and significant variation of NO_2^-, ranging from 0.2 to 1291 ng m^{-3} in air and with an average of 375 ± 386 ng m^{-3}. In comparison, NO_2^- consistently remained below the detection limit in $PM_{2.5}$ samples. Note during the laboratory measurements of ionic concentrations, TSP and $PM_{2.5}$ filters were extracted with ultrapure water and it was the extraction analyzed by ion chromatography. To ensure fair comparisons, similar areas of filters were extracted with same volume of ultrapure water, so that the extractions from the $PM_{2.5}$ filters should be more concentrated in atmospheric particulate species compared to that from the TSP filters, since $PM_{2.5}$ samples were collected at a much faster sampling speed (1.5 m^3 min^{-1} vs. 30 L min^{-1}) over the same sampling duration. Nevertheless, NO_2^- was detectable only in the extractions of TSP filter. The determined NO_2^- concentrations in TSP in this study (375 ± 386 ng m^{-3}) were higher than previous reports conducted in various remote sites, such as at QOMS station (~ 60 ng m^{-3} for TSP) (Bhattarai et al., 2023), at a forest site in the Southeast Tibet Plateau (~ 140 ng m^{-3} for TSP) (Bhattarai et al., 2019), in the middle hills of the central Himalayas (~ 210 ng m^{-3} for TSP) (Tripathee et al., 2021).

In particular, there was a dramatic decrease in TSP NO_2^- after 30 April, from a mean of (625 ± 457) to (147 ± 145) ng m^{-3}, in line with the declines in other secondary inorganic species. Over the course of the campaign, NO_2^- comprised approximately 8 % of the total WSIs mass in TSP, while its contribution reached maximum of ~ 20 % on 27 and 28 April, being one of the most abundant components on the 2 d. In addition, there was a strong correlation between NO_2^- and NO_3^- throughout the campaign ($r = 0.75$, $p < 0.05$, Fig. S3). Meanwhile, the mean mass ratio of NO_2^- to NO_3^- was ~ 50 % throughout the campaign, but on several days (i.e., night of 27 April) NO_2^- concentrations significantly exceeded that of NO_3^- (802 vs. 663 ng m^{-3}). Previous study also reported comparable NO_2^- and NO_3^- concentrations in at a forest site in the Southeast Tibet (summer: 100 vs. 110 ng m^{-3}; winter: 180 vs. 270 ng m^{-3}) (Bhattarai et al., 2019).

3.2 Isotopic signatures of nitrite in TSP

Figure 4 presents the times series of $\delta^{15}N$, $\delta^{18}O$ and $\Delta^{17}O$ of NO_2^- in TSP, along with the NO_2^- concentrations. Similar to the variation trend of NO_2^- concentrations, NO_2^- isotopes varied in a wider range before 30 April, but became more stable afterward. For example, $\delta^{15}N(NO_2^-)$ ranged from -10.9 ‰ to 0.8 ‰, with a relatively large standard deviation before 30 April compared to that after 30 April ((-6.4 ± 4.3) ‰ vs. (-8.0 ± 0.7) ‰). The large variability in $\delta^{15}N(NO_2^-)$ before 1 May is predominately attributed to the two high values observed in daytime of 27 April and night of 28 April. Note that the two high $\delta^{15}N(NO_2^-)$ samples were also associated with relatively high NO_2^- mass concentrations. In contrast to the declining trend of NO_2^- concentrations, the mean $\delta^{15}N(NO_2^-)$ values were comparable before and after 30 April. Relatively large variability was observed in TSP $\delta^{18}O(NO_2^-)$, ranging from -9.0 ‰ to 3.9 ‰

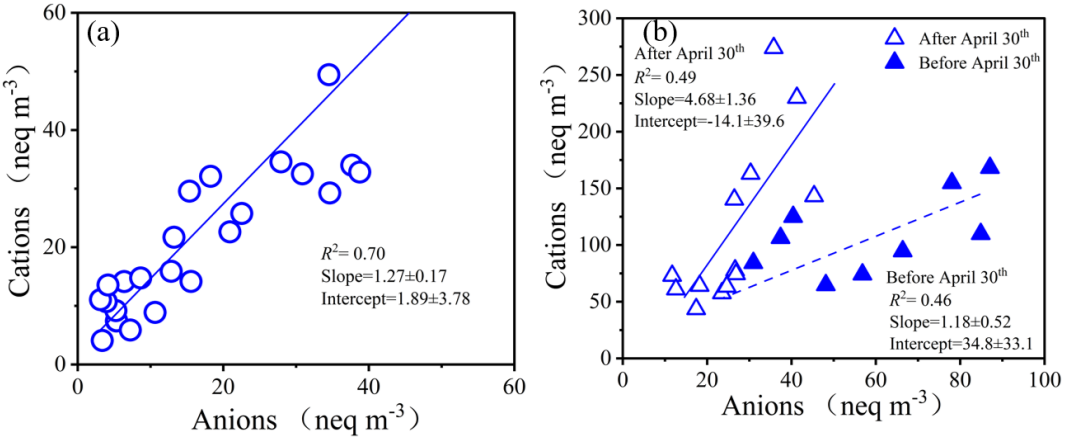

Figure 3. Ion balance for $PM_{2.5}$ (**a**, blue circles) and TSP samples (**b**, blue hollow triangles: samples collected after 30 April; blue solid triangles: samples collected before 30 April). Concentrations are expressed in nanogram-equivalent weight per cubic meter (neq m^{-3}).

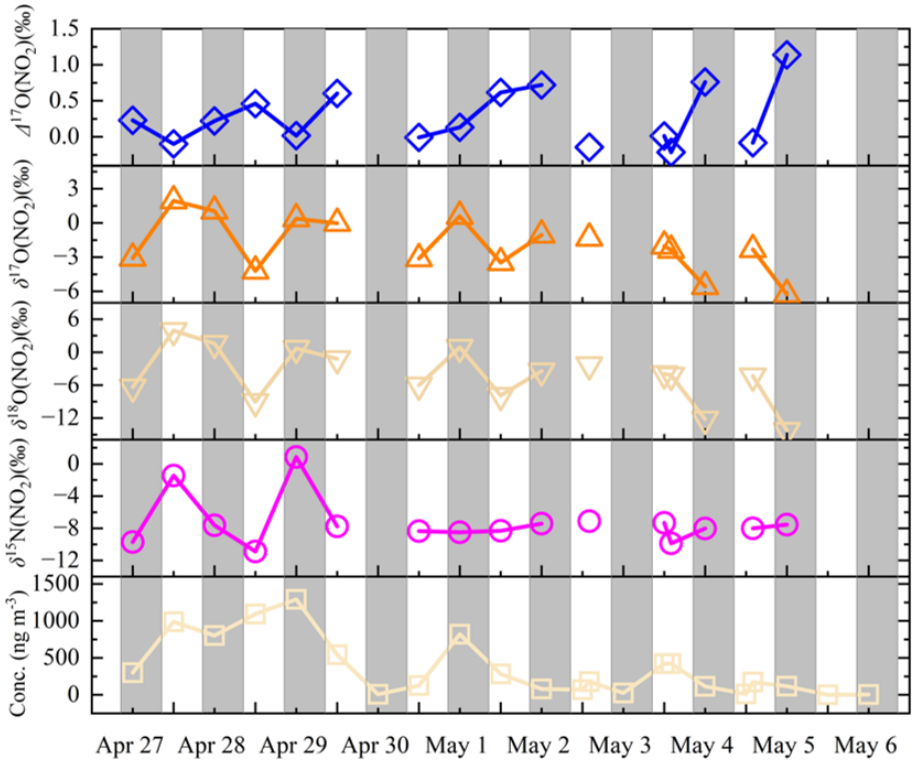

Figure 4. Time series of multiple isotopic signatures of NO_2^- ($\delta^{15}N$, $\delta^{18}O$, $\delta^{17}O$ and $\Delta^{17}O$) as well as corresponding concentrations in TSP samples during "Earth Summit Mission" scientific expedition in spring 2022. The gray shaded area denotes local nighttime.

and with an average of (-3.4 ± 3.8) ‰. TSP $\Delta^{17}O(NO_2^-)$ varied within a narrow range from -0.2 ‰ to $+0.7$ ‰ and with a mean of (0.2 ± 0.3) ‰. During the campaign, no significant correlations were observed between $\delta^{15}N(NO_2^-)$ and the NO_2^- concentrations; while $\delta^{18}O(NO_2^-)$ appeared to be moderately correlated with the NO_2^- concentrations (Fig. S5).

3.3 Surface soil nitrite concentration and isotopic signature

The concentration of soil NO_2^- (and NO_3^-) as well as the corresponding isotopic signatures are displayed in Table 1. The soil NO_2^- content on the west slope of Rongbuk Valley (on average 124.7 ng g^{-1}) was higher than that observed on the east and south sides (75.3 and 48.3 ng g^{-1}, respectively). The mean surface soil NO_2^- and NO_3^- in

Table 1. The measured nitrite (and nitrate) concentration and isotopic signatures in surface soil collected in the Rongbuk Valley.

Soil sample ID	NO_2^-				NO_3^-			
	Conc. ($ng\,g^{-1}$)	$\delta^{15}N$	$\delta^{18}O$	$\Delta^{17}O$	Conc. ($ng\,g^{-1}$)	$\delta^{15}N$	$\delta^{18}O$	$\Delta^{17}O$
East-1	67.7	−12.0	6.1	3.3	1127.3	−2.7	23.4	5.7
East-2	76.1	−11.9	2.7	2.2	1098.3	1.3	18.1	3.8
East-3	82.3	−14.6	6.0	3.3	2978.1	−0.3	25.4	6.6
West-1	88.6	−10.1	8.9	1.6	3176.5	−3.1	44.5	13.4
West-2	106.2	−7.0	11.4	1.5	2880.3	−1.2	22.1	6.2
West-3	179.3	−5.2	12.7	1.4	7686.9	−3.4	35.8	11.4
South-1	53.8	−13.2	12.7	6.7	3651.2	−0.6	32.6	10.1
South-2	42.3	−9.0	18.1	7.3	1683.2	−2.2	49.3	14.8
South-3	48.9	−10.3	12.4	6.7	385.5	−2.4	45.7	14.9

the Rongbuk Valley were 82.8 and 2740.8 $ng\,g^{-1}$, respectively. The soil NO_3^- concentrations were significantly higher than the NO_2^- by a factor of ∼ 8–40. In general, the measured soil NO_3^- concentrations at the Rongbuk valley were significantly lower than other remote regions of TP (i.e., 23.1 $\mu g\,g^{-1}$ at Naqu, 8.4 $\mu g\,g^{-1}$ at Yangbajing), while soil NO_2^- concentrations were comparable to these reports (i.e., 90.3 $ng\,g^{-1}$ at Naqu, 131.2 $ng\,g^{-1}$ at Yangbajing) (Wang et al., 2019). Soil $\delta^{15}N(NO_2^-)$ values ranged from −13.2 ‰ to −5.2 ‰ (on average −10.4 ‰), which are comparable to TSP $\delta^{15}N(NO_2^-)$ (−7.3 ‰). In comparison, we observed positive soil $\delta^{18}O(NO_2^-)$ and $\Delta^{17}O(NO_2^-)$, ranging from 2.7 ‰ to 18.1 ‰ (on average 10.5 ‰) and 1.4 ‰ to 7.3 ‰ (on average 3.8 ‰), respectively, in contrast to the negative $\delta^{18}O(NO_2^-)$ and near-zero $\Delta^{17}O(NO_2^-)$ observed in TSP samples. The determined soil $\delta^{18}O(NO_2^-)$ is comparable to that in laboratory incubated soil (11.8 ‰–12.5 ‰) (Lewicka-Szczebak et al., 2021).

4 Discussion

The significant contrast in NO_2^- concentrations between TSP and $PM_{2.5}$ samples, as shown in Fig. 1, suggests that at the sampling site atmospheric NO_2^- overwhelmingly exists in coarse particles. This observation is consistent with previous studies across the TP, which also reported the absence of NO_2^- in fine mode particles ($PM_{2.5}$ and $PM_{1.0}$) using either online real-time instrument or offline filter sampling (Decesari et al., 2010; Xu et al., 2020, 2024; Zhao et al., 2020), while relatively high levels of TSP NO_2^- have been reported (Bhattarai et al., 2019, 2023; Tripathee et al., 2017). In general, the chemical sources of particle NO_2^- in the atmosphere encompass the uptake of HONO, particulate nitrate photolysis, and the NO_2-related reactions (i.e., photo-enhanced uptake of NO_2 on mineral dust, heterogeneous reaction of NO_2 on the surface of aerosol) (Nie et al., 2012; VandenBoer et al., 2014a; Chen et al., 2019; Shang et al., 2021), as summarized in Table 2. In addition to these in-situ atmospheric processes, growing evidence has revealed that long-range transport of atmospheric pollutants from South Asia also contributes considerably to aerosol loadings in TP in the spring (Kang et al., 2019; Bhattarai et al., 2023; Zhao et al., 2020), which may also bring nitrite along with other pollutants. Moreover, the lifting of surface dust can also contribute to the atmospheric coarse particles and significantly influence the chemical composition of TSP (Zhang et al., 2021a; Pokharel et al., 2019), and therefore soil nitrite could also be a potential source for TSP NO_2^-. In the following discussion, we examine the potential importance of the abovementioned processes to the observed high NO_2^- content in coarse particle and discern the most likely ones.

4.1 The potential effects of atmospheric chemistry on NO_2^- in TSP

Increasing evidence supports particulate nitrate photolysis as an important source of atmospheric HONO especially in pristine atmosphere, with NO_2^- serving as the intermediate in the subsequent gas-particle partition process (Andersen et al., 2023; Ye et al., 2016). In theory, particulate NO_2^- (and HONO) produced from particulate nitrate photolysis might be associated with extremely negative $\delta^{15}N$ values, due to the significant nitrogen isotopic fractionation effect during nitrate photolysis (Erbland et al., 2013; Frey et al., 2009). For example, NO_2^- in water of hypersaline ponds and soil of McMurdo Dry Valleys, Antarctica, produced from the NO_3^- photolysis, were characterized by significantly negative $\delta^{15}N$ values (< −80 ‰) (Peters et al., 2014). However, $\delta^{15}N(NO_2^-)$ in this study was only ∼ 2 ‰ lower than the $\delta^{15}N(NO_3^-)$ in TSP samples collected during this campaign (on average (−5.3 ± 3.3) ‰, Sect. S1) and that at the QOMS stations (annual average of (−5.1 ± 2.3) ‰) (Wang et al., 2020). The similarity in $\delta^{15}N$ isotopes between NO_2^- and NO_3^- suggests particulate nitrate photolysis is unlikely to be the primary source of the TSP NO_2^-.

Table 2. Particulate nitrite concentration and formation pathways/sources compiled in the literature.

Site	Period	NO_2^- Conc. (Mean, ng m^{-3})	Formation pathways/Sources	Reference
QOMS station	Apr 2017	60	Biomass burning emission transported from South Asia	Bhattarai et al. (2023)
Bakersfield, California	May–Jul 2010	150	HONO uptake on lofted alkaline soil particles.	VandenBoer et al. (2014a)
Jinan, China	Nov 2013–Jan 2014	2080	Heterogeneous reactions of NO_2	Wang et al. (2015)
Seoul, Korea	May–Jul 2005	1410	Heterogeneous reactions of NO_2	Song et al. (2009)
Shanghai, China	Jun 2020	210	Heterogeneous reactions of NO_2, reduction of NO_2 by S(IV)	Shang et al. (2021)
Mt. Heng, China	Apr 2009	2500	Surface TiO_2 photocatalysis of NO_2	Nie et al. (2012)

In addition to nitrate photolysis, the absorption of HONO on alkaline aerosols (i.e., lofted dust and road salt particles) can also result in accumulation of NO_2^- into the particle phase (VandenBoer et al., 2014a; Chen et al., 2019). For example, VandenBoer et al. (2014a) observed a synchronous enhancement of fine particle NO_2^- (as high as 730 ng m^{-3}) alongside the buildup of HONO (up to 1.37 ppbv) after sunset in an agricultural site (VandenBoer et al., 2014a). However, the levels of HONO in terrestrial background environments, typically on the order of dozens of pptv (Ye et al., 2023), are obviously too low to support the observed unexpectedly high levels of particulate NO_2^- (up to 1300 ng m^{-3}). What is more, previous studies indicated the HONO uptake predominately occurs on fine particles (Wang et al., 2015; Chen et al., 2019; Shang et al., 2021), while our observations indicated NO_2^- only exists in coarse particles.

The uptake of NO_2 on mineral dust has also been identified as a significant route for the formation of particulate NO_2^- or gas-phase HONO (Nie et al., 2012; Ndour et al., 2008). For example, Nie et al. (2012) found a significantly enhanced NO_2^- in coarse particle during daytime in a dust storm event in Mt. Heng (up to 4.5 µg m^{-3}) (Nie et al., 2012). The proposed mechanism is initiated by photo-enhanced conversion of NO_2 to NO_2^- via photo-produced electrons on surface of dust. Nevertheless, given the relatively small NO_2 uptake coefficients on mineral dust or salt surface (generally lower than 1×10^{-6}) (Yu et al., 2021; Bao et al., 2022; Xuan et al., 2025) and the low concentration of NO_2 in pristine environment of TP (e.g., ∼ 140 pptv at Namco (Wang et al., 2023), and would be even lower at Mt. Qomolangma), such high levels of particulate NO_2^- are beyond the capacity of NO_2 heterogeneous reactions.

Other than the above-mentioned rationales, the atmospheric physicochemical processes leading to NO_2^- production would influence both fine and coarse-mode particles, and some of the processes (e.g., HONO uptake) preferentially interact with fine-mode particles. However, the observation indicated NO_2^- only exists in TSP but not $PM_{2.5}$, suggesting atmospheric physicochemical processes are unlikely to account for the elevated levels of NO_2^- in TSP.

4.2 Potential effect of atmospheric pollutants in South Asia via long-range transport

There is a growing body of compelling evidence indicating that the elevated aerosol loadings and some chemical species in TP during spring, i.e., black carbon (Cong et al., 2015; Kang et al., 2019) and soluble components (Dasari et al., 2023; Bhattarai et al., 2023; Lin et al., 2021; Wang et al., 2020; Zhao et al., 2020) are significantly linked to biomass burning emissions from South Asia, which can penetrate into TP via long range transport. Recently, Bhattarai et al. (2023) observed synchronously elevated water-soluble nitrogen compounds (i.e., NO_2^-, NH_4^+, NO_3^-), levoglucosan (a molecule marker for biomass burning) and bulk $\delta^{15}N$ signatures in TSP at QOMS station, once upon the arrival of biomass burning plumes from South Asia (Bhattarai et al., 2023). Specially, they found that TSP NO_2^- averaged 60 ng m^{-3} during the spring biomass burning influenced episodes, while NO_2^- was always below the detection limit in other seasons (Bhattarai et al., 2023). This suggests

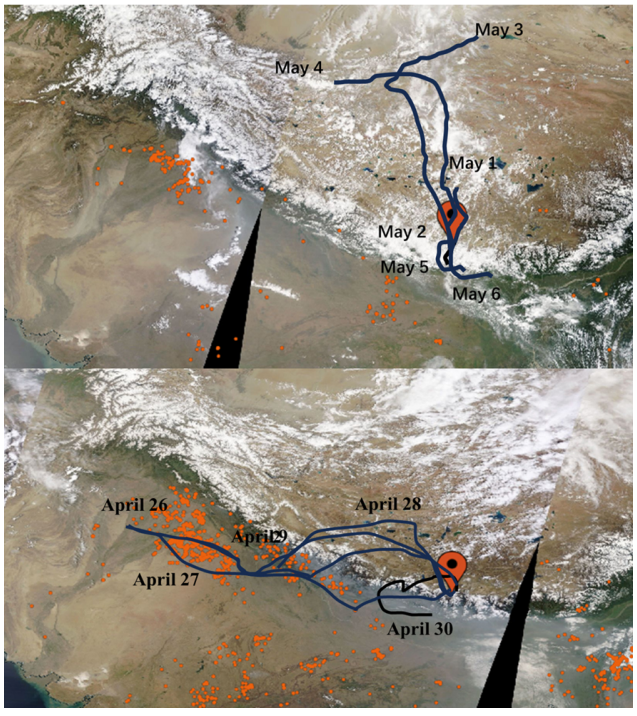

Figure 5. The modelled air-mass back trajectories during "Earth Summit Mission" scientific expedition in spring 2022 (**a**: from 1 to 6 May; **b**: 26 to 30 April). The active fire spots captured by MODIS (https://worldview.earthdata.nasa.gov, last access: 7 September 2024), the red dots in the figure) are also presented.

that biomass burning events in South Asia and the subsequent long-range transport could contribute to the accumulation of NO_2^- in aerosols in Tibet.

In this study, the mass concentrations and compositions of water-soluble ions, including SO_4^{2-}, NO_3^-, NH_4^+ and TSP NO_2^-, also varied substantially throughout the springtime campaign (Fig. 1). The potential effect of South Asian pollutants on our observations was explored by analyzing the air masses origins during the sampling period. As shown in Fig. 5, during the first-half of the campaign (i.e., before 30 April), air masses predominately originated from or passed through northern India and Nepal with intensive human activities and numerous fire hotspots (represented by the dense red dots in Fig. 5), indicating the potential impact of South Asia pollutants on aerosol loadings of TP. Correspondingly, elevated concentrations of secondary inorganic ions (i.e., NH_4^+, NO_3^- and SO_4^{2-}) in TSP and $PM_{2.5}$ were observed before 30 April, which are comparable to the values of previous reports in QOMS station when arrived air masses experiencing severe biomass burning emissions (Bhattarai et al., 2023; Lin et al., 2021). Meanwhile, elevated levels of TSP NO_2^- ($625 \pm 457\,ng\,m^{-3}$) was observed during this biomass burning-impacted period, and $\delta^{15}N(NO_2^-)$ values exhibited substantial variability. TSP samples collected during daytime of 27 April and night of 28 April were associated with high NO_2^- concentrations and $\delta^{15}N(NO_2^-)$ values. In comparison, TSP NO_2^- in other samples were significantly ^{15}N-depleted. Assuming that biomass burning emission accounted for the two high $\delta^{15}N(NO_2^-)$ samples (Bhattarai et al., 2023), the observed relatively low $\delta^{15}N(NO_2^-)$ in other samples before 30 April likely indicated the potential contribution from additional emission sources.

From 1 to 6 May, air masses originated primarily from the inside of the TP or surroundings and none of the fire hotspot was detected at the whole TP and along the air mass trajectories (Fig. 5), potentially excluding the influence of biomass burning and anthropogenic emissions during this period. Accompanied by this significant shift in air mass origins, the concentrations of NH_4^+, NO_3^- and SO_4^{2-} in both $PM_{2.5}$ and TSP, as well as the TSP NO_2^- apparently decreased. In particular, NH_4^+ in most $PM_{2.5}$ and TSP samples were below the detection limit during this period. Furthermore, K^+ in $PM_{2.5}$, a common tracer for biomass burning, declined from $269 \pm 432\,ng\,m^{-3}$ before 30 April to $22 \pm 12\,ng\,m^{-3}$ after 30 April, with the difference being statistically significant ($p < 0.05$). Meanwhile, the average TSP NO_2^- also declined significantly from $625 \pm 457\,ng\,m^{-3}$ before 30 April to $147 \pm 145\,ng\,m^{-3}$ after 30 April. Note substantially high levels of TSP NO_2^- were also observed on several days after 30 April, i.e., during daytime of 3 May ($\sim 400\,ng\,m^{-3}$). Although the TSP NO_2^- concentrations varied in wide range after 30 April, the $\delta^{15}N(NO_2^-)$ was relatively stable and comparable to that determined before 30 April (except for the two high $\delta^{15}N(NO_2^-)$ samples).

In short summary, these results likely suggest the significant impact of South Asia pollutants (i.e., biomass burning emissions) through long-range transport on the TSP NO_2^-, especially for samples collected before 30 April. However, it is difficult for the long-range transport to explain why NO_2^- is predominately present in coarse particles, as fine mode particle is typically easier to be transported in principle. While further studies need to be conducted to find out the exact reasons, one possibility is that the size partition of fine particle NO_2^- toward the coarse mode range during transport. Similar size shifts of NO_3^- have been observed and used to explain the enrichment of NO_3^- in coarse-mode aerosols in marine environment (Matsumoto et al., 2009). In addition, the coarse mode particles in this study contain more alkaline species (Fig. 2), which makes nitrite more stable in TSP during the transport or more stably exist in TSP after being uptake when the polluted air masses reaching TP. For the period after 30 April, since air masses originated from clean regions with little to no biomass burning sources, other sources of nitrite might be required.

4.3 The potential effects of lofted dust

Previous reports have confirmed that wind-blown mineral dust contributed significantly to coarse mode aerosols in TP (Kang et al., 2016; Zhang et al., 2021a). Notably, surface soil

collected from the Rongbuk valley is characterized with elevated NO_2^- concentration (up to 180 ng g^{-1}, Table 1). The surface soil NO_2^- is expected to mainly reside in the coarse mode after suspended in the atmosphere (Drakaki et al., 2022), consistent with our observations that particle NO_2^- was predominately confined into coarse particle. The unique environment of Rongbuk valley, characterized by exposed surface soil and strong wind (reaching as high as 9 m s^{-1} during this campaign) could facilitate the resuspension of soil components into the atmosphere. Furthermore, small localized tornadoes were frequently observed before 30 April, while the snow events occurred in 30 April would reduce the soil-derived dust emission by increasing the snow coverage and enriching the soil moisture. In fact, concentrations of Ca^{2+} in TSP, which predominately originate from dust emission, also declined to some extent after 30 April.

In addition, the comparable $\delta^{15}N$ values of NO_2^- between TSP collected after 1 May (-8.0 ± 0.7 ‰) and the surface soil (-10.3 ± 3.0 ‰) also supports that locally emitted surface soil is an important contributor to the observed high levels of TSP NO_2^-. But one should note that the oxygen isotopes ($\delta^{18}O$ and $\Delta^{17}O$) of TSP NO_2^- were significantly lower compared to that in soil NO_2^-, indicating that the original soil NO_2^- oxygen isotope may have been modified after resuspension. This discrepancy could be explained by the potential oxygen isotope exchanges between TSP NO_2^- and aerosol liquid water (fractionation effect of $^{18}\varepsilon_{eq} \approx 16$ ‰ at local temperature, $T = 270$ K, $^{18}\varepsilon_{eq} = -0.12T + 48.79$ (Buchwald and Casciotti, 2013)), which tend to deplete both the initial $\delta^{18}O(NO_2^-)$ and $\Delta^{17}O(NO_2^-)$.

We noted the oxygen isotope exchange process between NO_2^- and H_2O also occurs in surface soil. Previous study indicated that in high-altitude arid regions of TP (i.e., > 5000 m), denitrification process dominated the surface soil NO_2^- production, accounting for ~ 75 % (Wang et al., 2019). Soil NO_2^- generated from denitrification process is expect to inherit the $\Delta^{17}O$ signatures of substrate NO_3^-. In this study, the surface soil $\Delta^{17}O(NO_3^-)$ were positive with average values of 9.6 ‰ (Table 1). The positive soil $\Delta^{17}O(NO_3^-)$ have been observed on arid environments (Wang et al., 2016), such as desert soil, where the low water moisture favors the preservation of atmospherically derived NO_3^-. One could estimate that soil $\Delta^{17}O(NO_2^-)$ derived from the denitrification would be 9.6 ‰, nitrite from other sources (e.g., nitrification) should possess zero $\Delta^{17}O$, thus in total nitrite in soil should possess $\Delta^{17}O$ of ~ 7.2 ‰ (estimated as $0.75 \times \Delta^{17}O(NO_3^-)$). However, the determined soil $\Delta^{17}O(NO_2^-)$ (3.8 ‰) is significantly lower compared to the estimated soil $\Delta^{17}O(NO_2^-)$, indicating the occurrence of exchange process between soil water and NO_2^-, which would reduce the soil $\Delta^{17}O(NO_2^-)$ to some extent. The exchange process between soil water and NO_2^- is particularly evident in west slope of Rongbuk Valley, where soil $\Delta^{17}O(NO_2^-)$ is as low as 1.5 ‰ while soil $\Delta^{17}O(NO_3^-)$ is on average 10.3 ‰. Soil $\Delta^{17}O(NO_2^-)$ should be erased to near-zero if exchange process between soil water and NO_2^- was efficient. Therefore, the fact that the observed soil $\Delta^{17}O(NO_2^-)$ remain above 0 ‰ indicates unfavorable conditions for the oxygen isotope exchange process, likely due to the extremely low soil moisture content (~ 1 %) in surface soil (Ma et al., 2023).

Upon resuspension into atmosphere, the soil-derived dust aerosols usually exhibited a certain degree of hygroscopicity (Tang et al., 2016; Chen et al., 2020), allowing the absorption of water molecule on dust aerosol. For example, the aerosol water was determined to account for ~ 20 % of the total PM_{10} mass during Saharan dust plumes (Cardoso et al., 2018). Based on laboratory experiment, Tang et al. (2019) reported that Asian dust also exhibited substantial hygroscopic property and revealed that the water-soluble inorganic ions, such as Cl^-, SO_4^{2-} and NO_3^- played a critical role in the absorption of water molecules on dust aerosol (Tang et al., 2019). In the present study, the SO_4^{2-} and NO_3^- account for ~ 30 % of the total mass of water-soluble ions in TSP, implying the potential uptake of water vapor on aerosol surface. In addition to water-soluble ions, the hygroscopicity of mineral dust also depends on the surface areas, and wind-blown dust experiences a substantial increase in surface area after being lifted into the atmosphere, enhancing its capacity for water uptake (Chen et al., 2020; Seisel et al., 2004). The hygroscopicity of dust aerosol is expected to accelerate the oxygen isotope exchanges between NO_2^- and aerosol liquid water. The atmospheric water vapor $\delta^{18}O$ isotope in TP is determined to be significantly negative (approximately -35 ‰ to -15 ‰ at a remote site in TP with altitude of ~ 4200 m) (Yu et al., 2015). Similarly, the oxygen isotope exchange between NO_2^- and H_2O would also homogenize and erase original soil $\Delta^{17}O(NO_2^-)$ signals, because aerosol liquid water is characterized by negligible $\Delta^{17}O$ values (Luz and Barkan, 2005). Consequently, isotope exchange with aerosol water would further reduce both $\delta^{18}O$ and $\Delta^{17}O$ of TSP NO_2^-, effectively masking the original isotopic signature inherited from surface soil.

We also noted that NO_2^- in surface soil is significantly lower than NO_3^-, by on average 35 times (Table 1), contrasting with the chemical compositions in TSP. It is important to note that during the complex dust generation and aerosolization processes, water-soluble ions exhibit significant chemical enrichment relative to that in parent soil (Wu et al., 2022; Gao et al., 2023). For example, Wu et al. (2022) reported that contents of nitrate in sand dust-derived PM_{10} is higher than the original soil samples by ~ 2–80 times, while sulphate can be up to 500 times higher than the original soil. Although the enrichment of nitrite has not been evaluated to the extent of our knowledge, we propose that the observed discrepancy of nitrate / nitrite ratio between TSP and surface soil can be reconciled if the nitrite is enriched more efficiently than nitrate during dust aerosolization, i.e., by a factor of 30. To further assess the potential contribution of resuspended soil to elevated nitrite in TSP, we conducted a rough estimation based on laboratory inves-

tigations from Wu et al. (2022). First, the springtime TSP concentrations observed in the nearby QOMS station is used ($65.1 \pm 50.9\,\mu g\,m^{-3}$; Liu et al., 2017), as TSP mass concentrations surrounding the Base camp were not available. Second, we assume the nitrite content in soil-derived coarse particles to be similar to that of nitrate (0.2 %) in laboratory-generated dust aerosol from natural sandy and gravel soils (Wu et al., 2022), which is comparable to the soil texture of the Rongbuk Valley. This assumption can also explain the comparable amounts of nitrite and nitrate observed in TSP samples in this study. Results shown that the concentrations of nitrite in TSP can be approximately $130 \pm 102\,ng\,m^{-3}$, on the same order with the observed nitrite concentration in TSP after 30 April ($147 \pm 145\,ng\,m^{-3}$) but substantially lower than that before 30 April ($625 \pm 457\,ng\,m^{-3}$). Therefore, we speculate that the resuspension of surface soil may account for the observed TSP nitrite after 30 April, whereas the biomass burning and soil together co-contributed to the high TSP nitrite before 30 April. This is also consistent with the shift of air mass origins, which clearly indicated that airmasses before 30 April is significantly impacted by the biomass burning emissions, and after 30 April airmasses primarily originated from clean regions. While we acknowledge that this simplistic estimation is subject to substantial uncertainty, it provides a first-order assessment supporting the hypothesis that wind-blown soil dust contributes to coarse-mode particulate nitrite. Previously, wind-blown mineral dust has been verified as a potential source for aerosol water-soluble ions (Engelbrecht et al., 2016; Wu et al., 2022, 2012) and dust aerosol is also recognized as one of the important aerosol types over TP (Pokharel et al., 2019).

5 Conclusion and Implications

Unexpectedly high levels of NO_2^- associated with coarse-particle were observed in the pristine environment at Mt. Qomolangma in the spring, 2022. After examining the potential contributions of various NO_2^- sources with assistance from air mass back-trajectory and isotope analyses, we propose that both soil-derived nitrite and long-range transport of pollutants from South Asia may contribute to coarse-particle NO_2^- during spring at Mt. Qomolangma. This is also consistent with previous reports showing that dust and biomass burning emissions through long-range transport from South Asia are the predominant contributors to the springtime aerosol loadings over TP (Zhao et al., 2020; Pokharel et al., 2019). The nitrite concentrations and isotopes further indicated that soil-derived nitrite likely serves as a baseline source of atmospheric NO_2^-, maintaining the background levels of TSP NO_2^- at this pristine site, reflected by the relatively stable isotopes when soil-derived nitrite predominated. In addition, air masses originating from South Asia would result in elevated levels of NO_2^- observed before 30 April by bringing additional biomass burning and anthropogenic pollutants, as evidenced by the more varied isotopes before 30 April compared to after that day when air mass origins shifted from South Asia to central and north Tibet. However, the detailed mechanisms of nitrite enriched on the coarse particle remain unknown and need further explorations.

In the atmosphere, photolysis of particle nitrite can produce OH radical and NO, the latter is essential for the formation of atmospheric oxidants and secondary aerosols. Moreover, the elevated levels of particle NO_2^- may serve as an important HONO source through the gas-to-particle partition process (VandenBoer et al., 2014a), and the thermodynamic equilibrium between particulate nitrite and HONO ([pN(III)] / [HONO] ratio) is primarily governed by the particle acidity and liquid water content (LWC) in theory (Fountoukis and Nenes, 2007; VandenBoer et al., 2014a; Chen et al., 2019). Based on the observed TSP NO_2^- and estimated ratio of [pN(III)] / [HONO] (from 4.8 to 10.6, Sect. S2 in the Supplement), we can estimate the potential level of atmospheric HONO if the partition ever occurs at this site (VandenBoer et al., 2014b), and result indicates HOHO would be at 8–15 pptv, on the same order with the observations at a central Tibetan site ($\sim$ 30 pptv at Namco; Wang et al., 2023). Given that TSP concentrations usually reach maximum during spring over TP, i.e., $65 \pm 51\,\mu g\,m^{-3}$ at the nearby QOMS station (Liu et al., 2017), our findings suggest that the coarse-particle may serve as a potential source of atmospheric HONO and NO_x assuming the TSP are associated with nitrite. Although the coarse-particle tend to deposit rapidly within hours, their potential to influence local atmospheric chemistry remains important to some extent, particularly considering the frequent dust events in TP (loose arid/semiarid surface, sparse vegetation, and strong winds; Long et al., 2025) and the ubiquity of long-range transport of biomass burning emissions from South Asia during this season. The impact of the TSP nitrite on the budget of NO_x, HONO and OH radicals especially in the background atmosphere could be investigated using regional or global atmospheric transport model, once the detailed mechanism regarding the sources and chemistry of TSP nitrite been elucidated. In summary, our results highlight the need for further investigation into the sources, partitioning, and chemical reactivity of aerosol-phase nitrite, particularly in the pristine Tibetan Plateau, where even small inputs of NO_x or HONO can disproportionately affect oxidant budgets and reactive nitrogen cycling.

Data availability. The data supporting the findings of this study are available in the archival repository at https://doi.org/10.6084/m9.figshare.28188320.v1 (Zhang and Geng, 2025).

Supplement. The supplement related to this article is available online at https://doi.org/10.5194/acp-25-10625-2025-supplement.

Author contributions. LG designed the research, interpreted the data; LG and ZZ prepared the manuscript with contributions from all co-authors; ZZ, YW, CY, TZ, CZ, ZJ, and PC, conducted the field sampling and laboratory measurements; LG, ZZ, and PC, acquired funding; LG, SK, and CY reviewed and edited the manuscript. All authors have given approval to the final version of the manuscript.

Competing interests. The contact author has declared that none of the authors has any competing interests.

Disclaimer. Publisher's note: Copernicus Publications remains neutral with regard to jurisdictional claims made in the text, published maps, institutional affiliations, or any other geographical representation in this paper. While Copernicus Publications makes every effort to include appropriate place names, the final responsibility lies with the authors. Also, please note that this paper has not received English language copy-editing.

Acknowledgements. We thank Yunhong Zhou for the help in air mass back trajectory analysis. The authors thank all researchers involved in the "Earth Summit Mission-2022" scientific expedition from Peking University, Hefei Institutes of Physical Science Anhui Institute of Optics and Fine Mechanics of Chinese Academy of Sciences, Minzu University of China.

Financial support. Z.Z. acknowledges financial support from the National Natural Science Foundation of China (awards 42273001 and 42494851) and the Key Research and Development Plan Project of Anhui Province (2022l07020032). L.G. acknowledges financial support from the National Natural Science Foundation of China (awards W2411030, 42371151, and 41871051), the National Key R&D Program of China (2022YFC3700701), and the Innovation Program for Quantum Science and Technology (2021ZD0303101). P.C. acknowledges financial support from the National Natural Science Foundation of China (award: 42371151).

Review statement. This paper was edited by Armin Sorooshian and reviewed by Junling Li and two anonymous referees.

References

Albertin, S., Savarino, J., Bekki, S., Barbero, A., and Caillon, N.: Measurement report: Nitrogen isotopes ($\delta^{15}N$) and first quantification of oxygen isotope anomalies ($\Delta^{17}O$, $\delta^{18}O$) in atmospheric nitrogen dioxide, Atmos. Chem. Phys., 21, 10477–10497, https://doi.org/10.5194/acp-21-10477-2021, 2021.

Andersen, S. T., Carpenter, L. J., Reed, C., Lee, J. D., Chance, R., Sherwen, T., Vaughan, A. R., Stewart, J., Edwards, P. M., Bloss, W. J., Sommariva, R., Crilley, L. R., Nott, G. J., Neves, L., Read, K., Heard, D. E., Seakins, P. W., Whalley, L. K., Boustead, G. A., Fleming, L. T., Stone, D., and Fomba, K. W.: Extensive field evidence for the release of HONO from the photolysis of nitrate aerosols, Sci. Adv., 9, eadd6266, https://doi.org/10.1126/sciadv.add6266, 2023.

Bao, F., Cheng, Y., Kuhn, U., Li, G., Wang, W., Kratz, A. M., Weber, J., Weber, B., Pöschl, U., and Su, H.: Key Role of Equilibrium HONO Concentration over Soil in Quantifying Soil–Atmosphere HONO Fluxes, Environ. Sci. Technol., 56, 2204–2212, https://doi.org/10.1021/acs.est.1c06716, 2022.

Bhattarai, H., Zhang, Y.-L., Pavuluri, C. M., Wan, X., Wu, G., Li, P., Cao, F., Zhang, W., Wang, Y., and Kang, S.: Nitrogen speciation and isotopic composition of aerosols collected at Himalayan forest (3326 m asl): seasonality, sources, and implications, Environ. Sci. Technol., 53, 12247–12256, https://doi.org/10.1021/acs.est.9b03999, 2019.

Bhattarai, H., Wu, G., Zheng, X., Zhu, H., Gao, S., Zhang, Y.-L., Widory, D., Ram, K., Chen, X., and Wan, X.: Wildfire-Derived Nitrogen Aerosols Threaten the Fragile Ecosystem in Himalayas and Tibetan Plateau, Environ. Sci. Technol., 57, 9243–9251, https://doi.org/10.1021/acs.est.3c01541, 2023.

Buchwald, C. and Casciotti, K. L.: Isotopic ratios of nitrite as tracers of the sources and age of oceanic nitrite, Nat. Geosci., 6, 308–313, https://doi.org/10.1038/ngeo1745, 2013.

Cardoso, J., Almeida, S. M., Nunes, T., Almeida-Silva, M., Cerqueira, M., Alves, C., Rocha, F., Chaves, P., Reis, M., Salvador, P., Artiñano, B., and Pio, C.: Source apportionment of atmospheric aerosol in a marine dusty environment by ionic/composition mass balance (IMB), Atmos. Chem. Phys., 18, 13215–13230, https://doi.org/10.5194/acp-18-13215-2018, 2018.

Casciotti, K. L., Böhlke, J. K., McIlvin, M. R., Mroczkowski, S. J., and Hannon, J. E.: Oxygen isotopes in nitrite: Analysis, calibration, and equilibration, Anal. Chem., 79, 2427–2436, https://doi.org/10.1021/ac061598h, 2007.

Chai, J., Miller, D. J., Scheuer, E., Dibb, J., Selimovic, V., Yokelson, R., Zarzana, K. J., Brown, S. S., Koss, A. R., Warneke, C., and Hastings, M.: Isotopic characterization of nitrogen oxides (NO_x), nitrous acid (HONO), and nitrate (pNO_3^-) from laboratory biomass burning during FIREX, Atmos. Meas. Tech., 12, 6303–6317, https://doi.org/10.5194/amt-12-6303-2019, 2019.

Chai, J., Dibb, J. E., Anderson, B. E., Bekker, C., Blum, D. E., Heim, E., Jordan, C. E., Joyce, E. E., Kaspari, J. H., Munro, H., Walters, W. W., and Hastings, M. G.: Isotopic evidence for dominant secondary production of HONO in near-ground wildfire plumes, Atmos. Chem. Phys., 21, 13077–13098, https://doi.org/10.5194/acp-21-13077-2021, 2021.

Chen, L., Peng, C., Gu, W., Fu, H., Jian, X., Zhang, H., Zhang, G., Zhu, J., Wang, X., and Tang, M.: On mineral dust aerosol hygroscopicity, Atmos. Chem. Phys., 20, 13611–13626, https://doi.org/10.5194/acp-20-13611-2020, 2020.

Chen, Q., Edebeli, J., McNamara, S. M., Kulju, K. D., May, N. W., Bertman, S. B., Thanekar, S., Fuentes, J. D., and Pratt, K. A.: HONO, Particulate Nitrite, and Snow Nitrite at a Midlatitude Urban Site during Wintertime, ACS Earth Space Chem., 3, 811–822, https://doi.org/10.1021/acsearthspacechem.9b00023, 2019.

Cong, Z., Kang, S., Kawamura, K., Liu, B., Wan, X., Wang, Z., Gao, S., and Fu, P.: Carbonaceous aerosols on the south edge of the Tibetan Plateau: concentrations, seasonality and sources, Atmos. Chem. Phys., 15, 1573–1584, https://doi.org/10.5194/acp-15-1573-2015, 2015.

Dasari, S., Paris, G., Pei, Q., Cong, Z., and Widory, D.: Tracing the origin of elevated springtime atmospheric sulfate on the southern

Himalayan-Tibetan plateau, Environ. Sci.-Advances, 2, 1110–1118, https://doi.org/10.1039/D3VA00085K, 2023.

Decesari, S., Facchini, M. C., Carbone, C., Giulianelli, L., Rinaldi, M., Finessi, E., Fuzzi, S., Marinoni, A., Cristofanelli, P., Duchi, R., Bonasoni, P., Vuillermoz, E., Cozic, J., Jaffrezo, J. L., and Laj, P.: Chemical composition of PM_{10} and PM_1 at the high-altitude Himalayan station Nepal Climate Observatory-Pyramid (NCO-P) (5079 m a.s.l.), Atmos. Chem. Phys., 10, 4583–4596, https://doi.org/10.5194/acp-10-4583-2010, 2010.

Drakaki, E., Amiridis, V., Tsekeri, A., Gkikas, A., Proestakis, E., Mallios, S., Solomos, S., Spyrou, C., Marinou, E., Ryder, C. L., Bouris, D., and Katsafados, P.: Modeling coarse and giant desert dust particles, Atmos. Chem. Phys., 22, 12727–12748, https://doi.org/10.5194/acp-22-12727-2022, 2022.

Engelbrecht, J. P., Moosmüller, H., Pincock, S., Jayanty, R. K. M., Lersch, T., and Casuccio, G.: Technical note: Mineralogical, chemical, morphological, and optical interrelationships of mineral dust re-suspensions, Atmos. Chem. Phys., 16, 10809–10830, https://doi.org/10.5194/acp-16-10809-2016, 2016.

Erbland, J., Vicars, W. C., Savarino, J., Morin, S., Frey, M. M., Frosini, D., Vince, E., and Martins, J. M. F.: Air–snow transfer of nitrate on the East Antarctic Plateau – Part 1: Isotopic evidence for a photolytically driven dynamic equilibrium in summer, Atmos. Chem. Phys., 13, 6403–6419, https://doi.org/10.5194/acp-13-6403-2013, 2013.

Fang, T., Guo, H., Verma, V., Peltier, R. E., and Weber, R. J.: $PM_{2.5}$ water-soluble elements in the southeastern United States: automated analytical method development, spatiotemporal distributions, source apportionment, and implications for heath studies, Atmos. Chem. Phys., 15, 11667–11682, https://doi.org/10.5194/acp-15-11667-2015, 2015a.

Fang, Y. T., Koba, K., Wang, X. M., Wen, D. Z., Li, J., Takebayashi, Y., Liu, X. Y., and Yoh, M.: Anthropogenic imprints on nitrogen and oxygen isotopic composition of precipitation nitrate in a nitrogen-polluted city in southern China, Atmos. Chem. Phys., 11, 1313–1325, https://doi.org/10.5194/acp-11-1313-2011, 2011.

Fang, Y., Koba, K., Makabe, A., Takahashi, C., Zhu, W., Hayashi, T., Hokari, A. A., Urakawa, R., Bai, E., and Houlton, B. Z.: Microbial denitrification dominates nitrate losses from forest ecosystems, P. Natl. Acad. Sci. USA, 112, 1470–1474, https://doi.org/10.1073/pnas.1416776112, 2015b.

Felix, J. D. and Elliott, E. M.: Isotopic composition of passively collected nitrogen dioxide emissions: Vehicle, soil and livestock source signatures, Atmos. Environ., 92, 359–366, https://doi.org/10.1016/j.atmosenv.2014.04.005, 2014.

Fountoukis, C. and Nenes, A.: ISORROPIA II: a computationally efficient thermodynamic equilibrium model for K^+–Ca^{2+}–Mg^{2+}–NH_4^+–Na^+–SO_4^{2-}–NO_3^-–Cl^-–H_2O aerosols, Atmos. Chem. Phys., 7, 4639–4659, https://doi.org/10.5194/acp-7-4639-2007, 2007.

Frey, M. M., Savarino, J., Morin, S., Erbland, J., and Martins, J. M. F.: Photolysis imprint in the nitrate stable isotope signal in snow and atmosphere of East Antarctica and implications for reactive nitrogen cycling, Atmos. Chem. Phys., 9, 8681–8696, https://doi.org/10.5194/acp-9-8681-2009, 2009.

Gao, Q., Zhu, S., Zhou, K., Zhai, J., Chen, S., Wang, Q., Wang, S., Han, J., Lu, X., Chen, H., Zhang, L., Wang, L., Wang, Z., Yang, X., Ying, Q., Zhang, H., Chen, J., and Wang, X.: High enrichment of heavy metals in fine particulate matter through dust aerosol generation, Atmos. Chem. Phys., 23, 13049–13060, https://doi.org/10.5194/acp-23-13049-2023, 2023.

Geng, L., Alexander, B., Cole-Dai, J., Steig, E. J., Savarino, J., Sofen, E. D., and Schauer, A. J.: Nitrogen isotopes in ice core nitrate linked to anthropogenic atmospheric acidity change, P. Natl. Acad. Sci. USA, 111, 5808–5812, https://doi.org/10.1073/pnas.1319441111, 2014.

Hastings, M. G., Sigman, D. M., and Lipschultz, F.: Isotopic evidence for source changes of nitrate in rain at Bermuda, J. Geophys. Res.-Atmos., 108, https://doi.org/10.1029/2003jd003789, 2003.

Homyak, P. M., Vasquez, K. T., Sickman, J. O., Parker, D. R., and Schimel, J. P.: Improving nitrite analysis in soils: Drawbacks of the conventional 2M KCl extraction, Soil Sci. Soc. Am. J., 79, 1237–1242, https://doi.org/10.2136/sssaj2015.02.0061n, 2015.

Hsu, S. C., Liu, S. C., Huang, Y. T., Chou, C. C., Lung, S. C., Liu, T. H., Tu, J. Y., and Tsai, F.: Long-range southeastward transport of Asian biosmoke pollution: Signature detected by aerosol potassium in northern Taiwan, J. Geophys. Res.-Atmos., 114, https://doi.org/10.1029/2009JD011725, 2009.

Jacobi, H.-W., Kleffmann, J. R., Villena, G., Wiesen, P., King, M., France, J., Anastasio, C., and Staebler, R.: Role of nitrite in the photochemical formation of radicals in the snow, Environ. Sci. Technol., 48, 165–172, https://doi.org/10.1021/es404002c, 2014.

Kang, S., Chen, P., Li, C., Liu, B., and Cong, Z.: Atmospheric aerosol elements over the inland Tibetan Plateau: Concentration, seasonality, and transport, Aerosol Air Qual. Res., 16, 789–800, https://doi.org/10.4209/aaqr.2015.05.0307, 2016.

Kang, S., Zhang, Q., Qian, Y., Ji, Z., Li, C., Cong, Z., Zhang, Y., Guo, J., Du, W., Huang, J., You, Q., Panday, A. K., Rupakheti, M., Chen, D., Gustafsson, Ö., Thiemens, M. H., and Qin, D.: Linking atmospheric pollution to cryospheric change in the Third Pole region: current progress and future prospects, National Science Review, 6, 796–809, https://doi.org/10.1093/nsr/nwz031, 2019.

Keck, L. and Wittmaack, K. J. A. E.: Effect of filter type and temperature on volatilisation losses from ammonium salts in aerosol matter, Atmos. Environ., 39, 4093–4100, https://doi.org/10.1016/j.atmosenv.2005.03.029, 2005.

Lau, W. K., Kim, M.-K., Kim, K.-M., and Lee, W.-S.: Enhanced surface warming and accelerated snow melt in the Himalayas and Tibetan Plateau induced by absorbing aerosols, Environ. Res. Lett., 5, 025204, https://doi.org/10.1088/1748-9326/5/2/025204, 2010.

Lewicka-Szczebak, D., Jansen-Willems, A., Müller, C., Dyckmans, J., and Well, R.: Nitrite isotope characteristics and associated soil N transformations, Sci. Rep., 11, 5008, https://doi.org/10.1038/s41598-021-83786-w, 2021.

Li, S. M.: Equilibrium of particle nitrite with gas phase HONO: Tropospheric measurements in the high Arctic during polar sunrise, J. Geophys. Res.-Atmos., 99, 25469–25478, https://doi.org/10.1029/94jd00620, 2012.

Lin, W., Zhu, T., Song, Y., Zou, H., Tang, M., Tang, X., and Hu, J.: Photolysis of surface O_3 and production potential of OH radicals in the atmosphere over the Tibetan Plateau, J. Geophys. Res.-Atmos., 113, https://doi.org/10.1029/2007jd008831, 2008.

Lin, Y. C., Zhang, Y.-L., Yu, M., Fan, M.-Y., Xie, F., Zhang, W.-Q., Wu, G., Cong, Z., and Michalski, G.: Formation mecha-

nisms and source apportionments of airborne nitrate aerosols at a Himalayan-Tibetan Plateau site: Insights from nitrogen and oxygen isotopic compositions, Environ. Sci. Technol., 55, 12261–12271, https://doi.org/10.1021/acs.est.1c03957, 2021.

Liu, B., Cong, Z., Wang, Y., Xin, J., Wan, X., Pan, Y., Liu, Z., Wang, Y., Zhang, G., Wang, Z., Wang, Y., and Kang, S.: Background aerosol over the Himalayas and Tibetan Plateau: observed characteristics of aerosol mass loading, Atmos. Chem. Phys., 17, 449–463, https://doi.org/10.5194/acp-17-449-2017, 2017.

Liu, X.-Y., Koba, K., Koyama, L. A., Hobbie, S. E., Weiss, M. S., Inagaki, Y., Shaver, G. R., Giblin, A. E., Hobara, S., and Nadelhoffer, K.: Nitrate is an important nitrogen source for Arctic tundra plants, P. Natl. Acad. Sci. USA, 115, 3398–3403, https://doi.org/10.1073/pnas.1715382115, 2018.

Long, H., Cheng, L., Yang, F., and Zhang, G.: Temperature regulates dust activities over the Tibetan Plateau, The Innovation, 6, 100840, https://doi.org/10.1016/j.xinn.2025.100840, 2025.

Lüthi, Z. L., Škerlak, B., Kim, S.-W., Lauer, A., Mues, A., Rupakheti, M., and Kang, S.: Atmospheric brown clouds reach the Tibetan Plateau by crossing the Himalayas, Atmos. Chem. Phys., 15, 6007–6021, https://doi.org/10.5194/acp-15-6007-2015, 2015.

Luz, B. and Barkan, E.: The isotopic ratios $^{17}O/^{16}O$ and $^{18}O/^{16}O$ in molecular oxygen and their significance in biogeochemistry, Geochim. Cosmochim. Ac., 69, 1099–1110, https://doi.org/10.1016/j.gca.2004.09.001, 2005.

Ma, Y., Weber, R., Lee, Y. N., Orsini, D., Maxwell-Meier, K., Thornton, D., Bandy, A., Clarke, A., Blake, D., and Sachse, G.: Characteristics and influence of biosmoke on the fine-particle ionic composition measured in Asian outflow during the Transport and Chemical Evolution Over the Pacific (TRACE-P) experiment, J. Geophys. Res.-Atmos., 108, https://doi.org/10.1029/2002JD003128, 2003.

Ma, Y., Xie, Z., Ma, W., Han, C., Sun, F., Sun, G., Liu, L., Lai, Y., Wang, B., and Liu, X.: QOMS: a comprehensive observation station for climate change research on the top of Earth, B. Am. Meteorol. Soc., 104, E563–E584, https://doi.org/10.1175/BAMS-D-22-0084.1, 2023.

Matsumoto, K., Minami, H., Uyama, Y., and Uematsu, M.: Size partitioning of particulate inorganic nitrogen species between the fine and coarse mode ranges and its implication to their deposition on the surface ocean, Atmos. Environ., 43, 4259–4265, https://doi.org/10.1016/j.atmosenv.2009.06.014, 2009.

Miller, D. J., Chai, J., Guo, F., Dell, C. J., Karsten, H., and Hastings, M. G. J. G. R. L.: Isotopic composition of in situ soil NO_x emissions in manure-fertilized cropland, Geophys. Res. Lett., 45, 12058–12066, https://doi.org/10.1029/2018GL079619, 2018.

Ming, J., Zhang, D., Kang, S., and Tian, W.: Aerosol and fresh snow chemistry in the East Rongbuk Glacier on the northern slope of Mt. Qomolangma (Everest), J. Geophys. Res.-Atmos., 112, https://doi.org/10.1029/2007JD008618, 2007.

Morin, S., Savarino, J. l., Frey, M. M., Yan, N., Bekki, S., Bottenheim, J. W., and Martins, J. M. F.: Tracing the Origin and Fate of NO_x in the Arctic Atmosphere Using Stable Isotopes in Nitrate, Science, 322, 730–732, https://doi.org/10.1126/science.1161910, 2008.

Ndour, M., D'Anna, B., George, C., Ka, O., Balkanski, Y., Kleffmann, J., Stemmler, K., and Ammann, M.: Photoenhanced uptake of NO_2 on mineral dust: Laboratory experiments and model simulations, Geophys. Res. Lett., 35, https://doi.org/10.1029/2007GL032006, 2008.

Nie, W., Wang, T., Xue, L. K., Ding, A. J., Wang, X. F., Gao, X. M., Xu, Z., Yu, Y. C., Yuan, C., Zhou, Z. S., Gao, R., Liu, X. H., Wang, Y., Fan, S. J., Poon, S., Zhang, Q. Z., and Wang, W. X.: Asian dust storm observed at a rural mountain site in southern China: chemical evolution and heterogeneous photochemistry, Atmos. Chem. Phys., 12, 11985–11995, https://doi.org/10.5194/acp-12-11985-2012, 2012.

Peters, B., Casciotti, K. L., Samarkin, V. A., Madigan, M. T., Schutte, C. A., and Joye, S. B.: Stable isotope analyses of NO_2^-, NO_3^-, and N_2O in the hypersaline ponds and soils of the McMurdo Dry Valleys, Antarctica, Geochim. Cosmochim. Ac., 135, 87–101, https://doi.org/10.1016/j.gca.2014.03.024, 2014.

Pokharel, M., Guang, J., Liu, B., Kang, S., Ma, Y., Holben, B. N., Xia, X. A., Xin, J., Ram, K., Rupakheti, D., Wan, X., Wu, G., Bhattarai, H., Zhao, C., and Cong, Z.: Aerosol Properties Over Tibetan Plateau From a Decade of AERONET Measurements: Baseline, Types, and Influencing Factors, J. Geophys. Res.-Atmos., 124, 13357–13374, https://doi.org/10.1029/2019jd031293, 2019.

Seisel, S., Lian, Y., Keil, T., Trukhin, M. E., and Zellner, R.: Kinetics of the interaction of water vapour with mineral dust and soot surfaces at $T = 298$ K, Phys. Chem. Chem. Phys., 6, 1926–1932, https://doi.org/10.1039/B314568A, 2004.

Shang, X., Kang, H., Chen, Y., Abdumutallip, M., Li, L., Li, X., Fu, H., Wang, X., Wang, L., and Wang, X.: $PM_{1.0}$-nitrite heterogeneous formation demonstrated via a modified versatile aerosol concentration enrichment system coupled with ion chromatography, Environ. Sci. Technol., 55, 9794–9804, https://doi.org/10.1021/acs.est.1c02373, 2021.

Song, C. H., Park, M. E., Lee, E. J., Lee, J. H., Lee, B. K., Lee, D. S., Kim, J., Han, J. S., Moon, K. J., and Kondo, Y.: Possible particulate nitrite formation and its atmospheric implications inferred from the observations in Seoul, Korea, Atmospheric Environment, 43, 2168–2173, https://doi.org/10.1016/j.atmosenv.2009.01.018, 2009.

Tang, M., Cziczo, D. J., and Grassian, V. H.: Interactions of Water with Mineral Dust Aerosol: Water Adsorption, Hygroscopicity, Cloud Condensation, and Ice Nucleation, Chem. Rev., 116, 4205–4259, https://doi.org/10.1021/acs.chemrev.5b00529, 2016.

Tang, M., Zhang, H., Gu, W., Gao, J., Jian, X., Shi, G., Zhu, B., Xie, L., Guo, L., and Gao, X.: Hygroscopic properties of saline mineral dust from different regions in China: Geographical variations, compositional dependence, and atmospheric implications, J. Geophys. Res.-Atmos., 124, 10844–10857, https://doi.org/10.1029/2019JD031128, 2019.

Tripathee, L., Kang, S., Rupakheti, D., Cong, Z., Zhang, Q., and Huang, J.: Chemical characteristics of soluble aerosols over the central Himalayas: insights into spatiotemporal variations and sources, Environ. Sci. Pollut. Res., 24, 24454–24472, https://doi.org/10.1007/s11356-017-0077-0, 2017.

Tripathee, L., Kang, S., Chen, P., Bhattarai, H., Guo, J., Shrestha, K. L., Sharma, C. M., Sharma Ghimire, P., and Huang, J.: Water-soluble organic and inorganic nitrogen in ambient aerosols over the Himalayan middle hills: Seasonality, sources, and transport pathways, Atmos. Res., 250, 105376, https://doi.org/10.1016/j.atmosres.2020.105376, 2021.

VandenBoer, T., Markovic, M., Sanders, J., Ren, X., Pusede, S., Browne, E., Cohen, R., Zhang, L., Thomas, J., and Brune, W.: Evidence for a nitrous acid (HONO) reservoir at the ground surface in Bakersfield, CA, during CalNex 2010, J. Geophys. Res.-Atmos., 119, 9093–9106, https://doi.org/10.1002/2013JD020971, 2014a.

VandenBoer, T. C., Young, C. J., Talukdar, R. K., Markovic, M. Z., Brown, S. S., Roberts, J. M., and Murphy, J. G.: Nocturnal loss and daytime source of nitrous acid through reactive uptake and displacement, Nat. Geosci., 8, 55–60, https://doi.org/10.1038/ngeo2298, 2014b.

Vicars, W. C. and Savarino, J.: Quantitative constraints on the ^{17}O-excess (Δ^{17}O) signature of surface ozone: Ambient measurements from 50° N to 50° S using the nitrite-coated filter technique, Geochim. Cosmochim. Ac., 135, 270–287, https://doi.org/10.1016/j.gca.2014.03.023, 2014.

Wang, F., Ge, W., Luo, H., Seo, J.-H., and Michalski, G.: Oxygen-17 anomaly in soil nitrate: A new precipitation proxy for desert landscapes, Earth Planet. Sc. Lett., 438, 103–111, https://doi.org/10.1016/j.epsl.2016.01.002, 2016.

Wang, J., Zhang, Y., Zhang, C., Wang, Y., Zhou, J., Whalley, L. K., Slater, E. J., Dyson, J. E., Xu, W., Cheng, P., Han, B., Wang, L., Yu, X., Wang, Y., Woodward-Massey, R., Lin, W., Zhao, W., Zeng, L., Ma, Z., Heard, D. E., and Ye, C.: Validating HONO as an Intermediate Tracer of the External Cycling of Reactive Nitrogen in the Background Atmosphere, Environ. Sci. Technol., 57, 5474–5484, https://doi.org/10.1021/acs.est.2c06731, 2023.

Wang, K., Hattori, S., Kang, S., Lin, M., and Yoshida, N.: Isotopic constraints on the formation pathways and sources of atmospheric nitrate in the Mt. Everest region, Environ. Pollut., 267, 115274, https://doi.org/10.1016/j.envpol.2020.115274, 2020.

Wang, L., Wen, L., Xu, C., Chen, J., Wang, X., Yang, L., Wang, W., Yang, X., Sui, X., and Yao, L.: HONO and its potential source particulate nitrite at an urban site in North China during the cold season, Sci. Total Environ., 538, 93–101, https://doi.org/10.1016/j.scitotenv.2015.08.032, 2015.

Wang, S., Liu, W., Zhao, S., Wang, C., Zhuang, L., Liu, L., Wang, W., Lu, Y., Li, F., and Zhu, G.: Denitrification is the main microbial N loss pathway on the Qinghai-Tibet Plateau above an elevation of 5000 m, Sci. Total Environ., 696, 133852, https://doi.org/10.1016/j.scitotenv.2019.133852, 2019.

Wang, Y. Q.: MeteoInfo: GIS software for meteorological data visualization and analysis, Meteorological Applications, 21, 360–368, https://doi.org/10.1002/met.1345, 2014.

Wang, Z., Akimoto, H., and Uno, I.: Neutralization of soil aerosol and its impact on the distribution of acid rain over east Asia: Observations and model results, J. Geophys. Res.-Atmos., 107, ACH 6-1–ACH 6-12, https://doi.org/10.1029/2001jd001040, 2002.

Wu, F., Zhang, D., Cao, J., Xu, H., and An, Z.: Soil-derived sulfate in atmospheric dust particles at Taklimakan desert, Geophys. Res. Lett., 39, https://doi.org/10.1029/2012GL054406, 2012.

Wu, F., Cheng, Y., Hu, T., Song, N., Zhang, F., Shi, Z., Hang Ho, S. S., Cao, J., and Zhang, D.: Saltation–sandblasting processes driving enrichment of water-soluble salts in mineral dust, Environ. Sci. Technol. Lett., 9, 921–928, https://doi.org/10.1021/acs.estlett.2c00652, 2022.

Xu, J., Hettiyadura, A. P. S., Liu, Y., Zhang, X., Kang, S., and Laskin, A.: Regional differences of chemical composition and optical properties of aerosols in the Tibetan Plateau, J. Geophys. Res.-Atmos., 125, e2019JD031226, https://doi.org/10.1029/2019JD031226, 2020.

Xu, J., Zhang, X., Zhao, W., Zhai, L., Zhong, M., Shi, J., Sun, J., Liu, Y., Xie, C., Tan, Y., Li, K., Ge, X., Zhang, Q., and Kang, S.: High-resolution physicochemical dataset of atmospheric aerosols over the Tibetan Plateau and its surroundings, Earth Syst. Sci. Data, 16, 1875–1900, https://doi.org/10.5194/essd-16-1875-2024, 2024.

Xuan, H., Liu, C., Zhang, P., Chu, B., Liang, L., Ma, Q., and He, H.: A Review of Laboratory Studies on the Heterogeneous Chemistry of NO_2: Mechanisms and Uptake Kinetics, J. Phys. Chem. A, 129, 815–835, https://doi.org/10.1021/acs.jpca.4c07943, 2025.

Yao, T., Thompson, L. G., Mosbrugger, V., Zhang, F., Ma, Y., Luo, T., Xu, B., Yang, X., Joswiak, D. R., and Wang, W.: Third pole environment (TPE), Environmental Development, 3, 52–64, https://doi.org/10.1016/j.envdev.2012.04.002, 2012.

Ye, C., Zhou, X., Pu, D., Stutz, J., Festa, J., Spolaor, M., Tsai, C., Cantrell, C., Mauldin, R. L., 3rd, Campos, T., Weinheimer, A., Hornbrook, R. S., Apel, E. C., Guenther, A., Kaser, L., Yuan, B., Karl, T., Haggerty, J., Hall, S., Ullmann, K., Smith, J. N., Ortega, J., and Knote, C.: Rapid cycling of reactive nitrogen in the marine boundary layer, Nature, 532, 489–491, https://doi.org/10.1038/nature17195, 2016.

Ye, C., Zhou, X., Zhang, Y., Wang, Y., Wang, J., Zhang, C., Woodward-Massey, R., Cantrell, C., Mauldin, R. L., Campos, T., Hornbrook, R. S., Ortega, J., Apel, E. C., Haggerty, J., Hall, S., Ullmann, K., Weinheimer, A., Stutz, J., Karl, T., Smith, J. N., Guenther, A., and Song, S.: Synthesizing evidence for the external cycling of NO_x in high- to low-NO_x atmospheres, Nat. Commun., 14, 7995, https://doi.org/10.1038/s41467-023-43866-z, 2023.

Yu, C., Wang, Z., Ma, Q., Xue, L., George, C., and Wang, T.: Measurement of heterogeneous uptake of NO_2 on inorganic particles, sea water and urban grime, J. Environ. Sci., 106, 124–135, https://doi.org/10.1016/j.jes.2021.01.018, 2021.

Yu, W., Tian, L., Ma, Y., Xu, B., and Qu, D.: Simultaneous monitoring of stable oxygen isotope composition in water vapour and precipitation over the central Tibetan Plateau, Atmos. Chem. Phys., 15, 10251–10262, https://doi.org/10.5194/acp-15-10251-2015, 2015.

Zhang, L., Tang, C., Huang, J., Du, T., Guan, X., Tian, P., Shi, J., Cao, X., Huang, Z., and Guo, Q.: Unexpected high absorption of atmospheric aerosols over a western Tibetan Plateau site in summer, J. Geophys. Res.-Atmos., 126, e2020JD033286, https://doi.org/10.1029/2020JD033286, 2021a.

Zhang, Y.-L., Zhang, W., Fan, M.-Y., Li, J., Fang, H., Cao, F., Lin, Y.-C., Wilkins, B. P., Liu, X., Bao, M., Hong, Y., and Michalski, G.: A diurnal story of $\Delta^{17}O(NO_3^-)$ in urban Nanjing and its implication for nitrate aerosol formation, npj Climate and Atmospheric Science, 5, 50, https://doi.org/10.1038/s41612-022-00273-3, 2022.

Zhang, Z. and Geng, L.: On the presence of high nitrite (NO2-) in coarse particles at Mt. Qomolangma.xls, figshare [data set], https://doi.org/10.6084/m9.figshare.28188320.v1, 2025.

Zhang, Z., Zeng, Y., Zheng, N., Luo, L., Xiao, H., and Xiao, H.: Fossil fuel-related emissions were the major source of NH_3 pollution in urban cities of northern China

in the autumn of 2017, Environ. Pollut., 256, 113428, https://doi.org/10.1016/j.envpol.2019.113428, 2020.

Zhang, Z., Jiang, Z., Guan, H., Liang, Y., Zheng, N., and Guo, W.: Isotopic evidence for the high contribution of wintertime photochemistry to particulate nitrate formation in Northern China, J. Geophys. Res.-Atmos., 126, e2021JD035324, https://doi.org/10.1029/2021jd035324, 2021b.

Zhang, Z., Zhou, T., Jiang, Z., Ma, T., Su, G., Ruan, X., Wu, Y., Cao, Y., Wang, X., Liu, Z., Li, W., Zhang, H., Lin, M., Liu, P., and Geng, L.: High-Resolution Measurements of Multi-Isotopic Signatures ($\delta^{15}N$, $\delta^{18}O$, and $\Delta^{17}O$) of Winter NO_2 in a Megacity in Central China, Environ. Sci. Technol., 59, 3634–3644, https://doi.org/10.1021/acs.est.4c07724, 2025.

Zhao, C., Yang, Y., Fan, H., Huang, J., Fu, Y., Zhang, X., Kang, S., Cong, Z., Letu, H., and Menenti, M.: Aerosol characteristics and impacts on weather and climate over the Tibetan Plateau, National Science Review, 7, 492–495, https://doi.org/10.1093/nsr/nwz184, 2020.

Zhou, L., Zou, H., Ma, S., Li, P., Zhu, J., and Huo, C.: Vertical air mass exchange driven by the local circulation on the northern slope of Mount Everest, Adv. Atmos. Sci., 28, 217–222, https://doi.org/10.1007/s00376-010-9231-z, 2011.

Zhou, T., Jiang, Z., Zhou, J., Zhao, W., Wu, Y., Yu, H., Li, W., Zhang, Z., Su, G., Ma, T., and Geng, L.: Fast and Efficient Atmospheric NO_2 Collection for Isotopic Analysis by a 3D-Printed Denuder System, Anal. Chem., 94, 13215–13222, https://doi.org/10.1021/acs.analchem.2c02839, 2022.

Zhu, T., Lin, W., Song, Y., Cai, X., Zou, H., Kang, L., Zhou, L., and Akimoto, H.: Downward transport of ozone-rich air near Mt. Everest, Geophys. Res. Lett., 33, https://doi.org/10.1029/2006GL027726, 2006.

Zong, Z., Sun, Z., Xiao, L., Tian, C., Liu, J., Sha, Q., Li, J., Fang, Y., Zheng, J., and Zhang, G.: Insight into the Variability of the Nitrogen Isotope Composition of Vehicular NO_x in China, Environ. Sci. Tech., 54, 14246–14253, https://doi.org/10.1021/acs.est.0c04749, 2020.

Zou, H., Zhou, L., Ma, S., Li, P., Wang, W., Li, A., Jia, J., and Gao, D.: Local wind system in the Rongbuk Valley on the northern slope of Mt. Everest, Geophys. Res. Lett., 35, https://doi.org/10.1029/2008gl033466, 2008.